Computational and Structural Biotechnology Journal 19 (2021) 3427–3436

COMPUTATIONAL AND STRUCTURAL BIOTECHNOLOGY JOURNAL

journal homepage: www.elsevier.com/locate/csbj

Zeta-carbonic anhydrases show CS_2 hydrolase activity: A new metabolic carbon acquisition pathway in diatoms?

Vincenzo Alterio [a,1], Emma Langella [a,1], Martina Buonanno [a], Davide Esposito [a], Alessio Nocentini [b], Emanuela Berrino [b], Silvia Bua [b], Maurizio Polentarutti [c], Claudiu T. Supuran [b], Simona Maria Monti [a,*], Giuseppina De Simone [a,*]

[a] Istituto di Biostrutture e Bioimmagini-CNR, via Mezzocannone 16, 80134 Napoli, Italy
[b] NEUROFARBA Department, Pharmaceutical and Nutraceutical Section, University of Firenze, Via Ugo Schiff 6, 50019 Sesto Fiorentino, Italy
[c] Elettra - Sincrotrone Trieste, s.s. 14 Km 163.5 in Area Science Park, Basovizza (Trieste) 34149, Trieste, Italy

ARTICLE INFO

Article history:
Received 16 April 2021
Received in revised form 27 May 2021
Accepted 30 May 2021
Available online 5 June 2021

Keywords:
Cambialistic enzyme
Carbonic Anhydrase
CO_2
CS_2
Molecular dynamics

ABSTRACT

CDCA1 is a very peculiar member of the Carbonic Anhydrase (CA) family. It has been the first enzyme to show an efficient utilization of Cd(II) ions in Nature and a unique adaptation capability to live on the surface ocean. Indeed, in this environment, which is extremely depleted in essential metal ions, CDCA1 can utilize Zn(II) or Cd(II) as catalytic metal to support the metabolic needs of fast growing diatoms. In this paper we demonstrate a further catalytic versatility of this enzyme by using a combination of X-ray crystallography, molecular dynamics simulations and enzymatic experiments. First we identified the CO_2 binding site and the way in which this substrate travels from the environment to the enzyme active site. Then, starting from the observation of a structural similarity with the substrate entry route of CS_2 hydrolase from *Acidanius A1-3*, we hypothesized and demonstrated that also CS_2 is a substrate for CDCA1. This finding is new and unexpected since until now only few CS_2 hydrolases have been characterized, and none of them is reported to have any CO_2 hydratase action. The physiological implications of this supplementary catalytic activity still remain to be unveiled. We suggest here that it could represent another ability of diatoms expressing CDCA1 to adapt to the external environment. Indeed, the ability of this enzyme to convert CS_2 could represent an alternative source of carbon acquisition for diatoms, in addition to CO_2.

1. Introduction

Carbonic anhydrases (CAs) are ubiquitous metallo-enzymes that catalyze the reversible hydration of CO_2 to bicarbonate ion and proton. These enzymes are present in organisms of all life kingdoms, where they are involved in many essential processes such as photosynthesis, CO_2 transport, pH regulation, and metabolic biosynthetic reactions [1]. Currently, eight genetic families, namely α-, β-, γ-, δ-, ζ-, η-, θ- and ι-class, have been identified, with little to no structural homology [2–8] and with some differences in their preference for metal ions involved in the catalytic reaction [1,2,8].

In all CA classes, the catalytic reaction follows a two-step mechanism, described by the equations (1) and (2). In the first step, a metal hydroxide species of the enzyme (EM^{2+}–OH^-) acts as a nucleophile on the CO_2 molecule, bound in a hydrophobic pocket in close proximity, with formation of HCO_3^-, which is then displaced from the active site by a water molecule (Eq. (1)), leading to the inactive form of the enzyme (EM^{2+}–H_2O). The second step regenerates the metal hydroxide species through a proton transfer reaction from the EM^{2+}-bound water molecule to an exogenous

Abbreviations: CDCA1, Cadmium-specific Carbonic Anhydrase; CA, Carbonic Anhydrase; CS_2H, *S. solfataricus* CS_2 hydrolase; bCA, bovine Carbonic Anhydrase; hCA, human Carbonic Anhydrase; psCA3, Pseudomonas aeruginosa Carbonic Anhydrase 3; FbiCA, Flaveria bidentis Carbonic Anhydrase; CAI, Carbonic Anhydrase Inhibitor; AAZ, Acetazolamide; DMSO, Dimethyl Sulfoxide; IPTG, Isopropyl-β-D-1-thiogalactopyranoside; Tris-HCl, Tris(hydroxymethyl)aminomethane hydrochloride; SDS-PAGE, Sodium Dodecyl Sulphate - PolyAcrylamide Gel Electrophoresis; HEPES, 2-[4-(2-hydroxyethyl)piperazin-1-yl]ethanesulfonic acid; PEG, Polyethylene glycol; MD, Molecular Dynamics; NCS, Non-Crystallographic Symmetry; PDB, Protein Data Bank; CCD, Charge Coupled Device.

* Corresponding authors.
E-mail addresses: marmonti@unina.it (S.M. Monti), giuseppina.desimone@cnr.it (G. De Simone).

[1] These authors contributed equally to the work.

https://doi.org/10.1016/j.csbj.2021.05.057

proton acceptor or to an active site residue, represented by B in Eq. (2).

$$EM^{2+} - OH^- + CO_2 \leftrightarrows EM^{2+} - HCO_3^- \overset{H_2O}{\leftrightarrows} EM^{2+} - H_2O + HCO_3^- \quad (1)$$

$$EM^{2+}—H_2O + B \leftrightarrows EM^{2+}—OH^- + BH^+ \quad (2)$$

This mechanism has been thoroughly characterized in the case of α- and β-CAs, with the clear identification of both CO_2 and bicarbonate binding sites [9–12] whereas much less data are available on the other CA families.

We recently focused our attention on the ζ-CAs. CDCA1 from the marine diatom *Thalassiosira weissflogii*, was the first enzyme of this class to be extensively characterized [2,13–18] showing rather peculiar features. In particular, this enzyme is a multidomain protein of 617 residues formed by three repeats (R1, R2 and R3) which share about 85% sequence identity [13], each one containing its own active site [2,13,16,19]. Kinetic analyses demonstrated that both the single repeats and full-length enzyme exhibit high CA activity with either Cd or Zn as catalytic metal, with slightly higher efficiency for the zinc-bound form [2]. The crystal structures of the three single repeats were also determined [2,14] showing a very similar 3D structure characterized by nine β-strands and seven α-helices. Seven out of the nine β-strands are positioned in the center of the structure forming two contiguous β-sheets. In each repeat, the active site is in a narrow cleft with the metal ion at the bottom, coordinated by three conserved protein residues (two cysteines and one histidine) and one water molecule in a tetrahedral geometry. In the case of the Cd-containing repeats, a second water molecule is bound to the metal ion [2]. Structural data highlighted a facile opening of the metal coordination site in the absence of metal ions, thus explaining the capability of the enzyme to exchange cadmium and zinc at its active site. Due to this feature, CDCA1 was classified as a cambialistic enzyme [2]. A model of the full-length protein was also obtained by docking approaches [14] showing a quite compact non symmetric structure, characterized by two covalently linked R1-R2 and R2-R3 interfaces and a small non-covalent R1-R3 interface [14].

Here we report a further characterization of this enzyme, identifying the CO_2 binding site and the entry route for the reaction substrate by a combined crystallographic and molecular dynamics approach. Results highlighted a similarity between the identified substrate entry route with that existing in a related enzyme, namely CS_2 hydrolase from *Acidianus* A1-3 [20]. This prompted us to investigate on the capability of CDCA1 to hydrate CS_2 to H_2S with COS as the intermediate. Biochemical assays confirmed this new and unexpected catalytic activity for CDCA1, which emerged as the only enzyme so far known able to use both CO_2 and CS_2 as substrates.

2. Materials and methods

2.1. Expression and purification of Zn-R3, Cd-R3 and CS_2H

The single R3 repeat containing in the active site either Zn^{2+} (Zn-R3) or Cd^{2+} (Cd-R3) was produced as previously described [14]. cDNA encoding *S. solfataricus* CS_2 hydrolase (P2 SS01214 gene product) (CS_2H) in pET-30a(+) (Novagen) was a kind gift from dr. Smeulders and prof. Op den Camp, Radboud University [20]. Expression in *E. coli* BL21 (DE3) cells was carried out in LB broth with 0.1 mM IPTG (isopropil-β-D-1-thiogalactopyranoside) for 16 h at 22 °C. Cells were harvested by centrifugation at 4 °C and resuspended in lysis buffer (20 mM Tris-HCl, 20 mM imidazole, 500 mM NaCl, pH 8.0), in presence of 1 mM phenylmethanesulfonyl fluoride, 5 mg/mL DNase I, 0.1 mg/mL lysozyme, 1 μg/mL Aprotinin, 1 μg/mL Leupeptin and 1 μg/mL Pepstatin protease inhibitors (Sigma-Aldrich). After sonication and centrifugation, the supernatant was purified on a 1 mL HisTrapHP column according to manufacturer's instruction (GE Healthcare) followed by a size exclusion chromatography in 20 mM Tris-HCl, 150 mM NaCl, pH 8.0. Protein purity was assessed by 15% SDS-PAGE using Biorad Precision Plus Protein All Blue Standards (10–250 kDa) as molecular mass marker.

2.2. X-ray crystallography

Zn-R3 fragment of CDCA1 was crystallized at 293 K using the hanging drop vapor diffusion technique. Crystals were obtained by mixing 1 μL of enzyme solution (10 mg/mL enzyme in 20 mM Tris-HCl pH 8.0, 150 mM sodium chloride) with an equal volume of a precipitant solution containing 27% (w/v) PEG 3350, 20 mM sodium dihydrogen phosphate, 100 mM HEPES pH 7.5, and equilibrating the drop over a well containing 1 mL of precipitant solution. Crystals appeared after 3 days and grew in about one week to maximum dimensions of 0.3 × 0.2 × 0.1 mm^3. Diffraction data were collected at 100 K to 1.98 Å resolution, using a Rigaku MicroMax-007 HF generator producing Cu Kα radiation and equipped with a Saturn 944 CCD detector. Before cryogenic freezing, crystals were transferred to the precipitant solution with the addition of 15% (w/v) glycerol.

Data were processed using the HKL2000 crystallographic data resolution package (Denzo/Scalepack) [21]. Crystals belonged to the C2 space group and the Matthews coefficient indicated the presence of two molecules in the asymmetric unit, according to a solvent content of 54%. The structure was solved by molecular replacement using the program AMoRe [22] and the coordinates of the Cd-R3/acetate complex (PDB 3UK8) [14] as starting model, and refined by using the program CNS [23,24]. An initial NCS-constrained refinement was carried out until R_{work}/R_{free} values reached 23.7/25.4%. Subsequently, the NCS constraints were removed, and the structure was further refined to final R_{work}/R_{free} values of 20.8/24.3%. After each refinement cycle, the σA weighted |2Fo-Fc| and |Fo-Fc| maps were calculated, and the model was rebuilt manually using the program O [25] guided by the electron density maps. Data collection and refinement statistics are summarized in Table S1. The two molecules in the asymmetric unit showed only minor differences, with an r.m.s.d for the superposition of the corresponding Cα atoms of only 0.3 Å. The two active sites were identical and therefore only one molecule has been arbitrarily chosen for the discussion.

Zn-R3/CO_2 complex was obtained by pressurizing Zn-R3 crystals with CO_2. For this purpose, Zn-R3 crystals where obtained following the procedure described above, but using as precipitant solution 28% (w/v) PEG 2000, 20 mM lithium sulfate, 100 mM sodium citrate pH 5.9. Before pressurization, crystals were transferred into a cryo-protectant solution containing 10% (v/v) glycerol. Subsequently, a drop containing one crystal was overlaid with paraffin oil, transferred to the pressurization device [26] and pressurized at 3 bar for 5 min. After pressurization, crystals were flash-cooled into liquid nitrogen within approximately 2 s from the release of pressure. A complete dataset was collected at 1.60 Å resolution, at synchrotron source Elettra in Trieste, using a PILATUS 2 M detector. Data were processed using the HKL2000 crystallographic data resolution package (Denzo/Scalepack) [21]. Crystals belonged to the C2 space group with two molecules in the asymmetric unit, according to a solvent content of 55%. Crystal parameters and data collection statistics are reported in Table S1. As for Zn-R3, the structure of Zn-R3/CO_2 complex was solved by molecular replacement using the program AMoRe [22] (the unbound structure was used as starting model) and refined by using CNS

[23,24] to final R_{work}/R_{free} values of 21.5/24.6%, following the same refinement protocol used for Zn-R3. Data refinement statistics are summarized in Table S1. After the initial cycles of crystallographic refinement, the |2Fo-Fc| and |Fo-Fc| maps clearly showed in the active site of both molecules in the asymmetric unit an ovoid electron density corresponding to the CO_2 molecule, which was then added to crystallographic coordinates for further refinement (Fig. 1). Surprisingly, the inspection of the |Fo-Fc| map revealed that the active site of molecule A contained in the position occupied in the unbound structure by the water molecule W1, a species with a higher molecular weight. Therefore, the zinc-bound solvent molecule in the active site of molecule A was substituted with a chloride ion, resulting in a good agreement with the electron density maps at the end of the refinement. For this reason, only molecule B has been considered for the discussion.

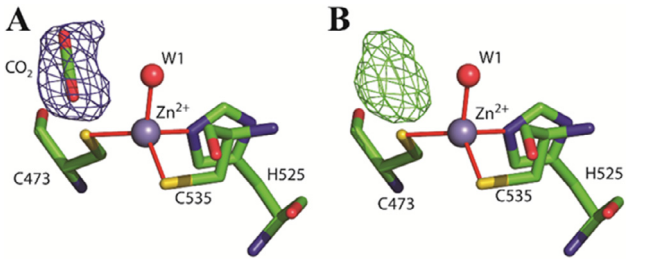

Fig. 1. Active site region of the Zn-R3/CO_2 adduct, showing σA-weighted |2Fo-Fc| map (contoured at 1.0 σ) relative to the CO_2 molecule (A) and σA-weighted |Fo-Fc| map (contoured at 3.0 σ) relative to the CO_2 molecule, obtained removing from the model the CO_2 molecule before refinement (B). Zn^{2+} coordination (red continuous lines) is also shown. (For interpretation of the references to colour in this figure legend, the reader is referred to the web version of this article.)

2.3. Molecular dynamics simulations and CAVER analysis

Two different Zn-R3/CO_2 systems were studied through MD simulations: one having the CO_2 molecule in the binding site of the protein (system A), and the other having CO_2 placed out of the protein (system B). In both cases, the crystallographic coordinates of the Zn-R3/CO_2 complex herein reported were used as starting structure, but in the case of system B the CO_2 coordinates were changed since the molecule was placed out of the protein at ~ 5 Å distance from the Zn-R3 tunnel opening (Fig. S1 in supplementary file). Crystallographic water molecules were deleted from the coordinate file, except that coordinating Zn^{2+} ion.

The systems were subjected to all-atom MD simulations using the GROMACS simulation package and Amber99SB-ILD force field [27]. Charges and force field parameters for CO_2 molecule were assigned according to GAFF (Generalised Amber Force Field) by using ACPYPE server [28]. The Zn-R3/CO_2 complexes were immersed in a dodecahedral box filled with water molecules (TIP3P water model) with a minimum distance of 11 Å between the protein and the box boundaries. Counter-ions (Na^+ or Cl^-) were added to neutralize the system (reaching a concentration of 0.1 M). Periodic boundary conditions were employed and the LINCS algorithm [29] was used to constrain bond lengths. The particle mesh Ewald method with a grid spacing of 1.6 Å was employed to treat electrostatic interactions [30] whereas for the Lennard-Jones potential a non-bonded cutoff of 10 Å was used [31]. Water molecules were relaxed by energy minimization using steepest descent for 10,000 steps. Equilibration of the systems was first conducted for 100 ps at 298 K temperature (NVT ensemble) and then for 100 ps at 1 atm pressure (NPT ensemble) with positional restraints on the protein. The V-rescale thermostat and Parrinello-Rahman barostat, were used for temperature and pressure control, respectively. After equilibration, the systems were simulated in NPT standard conditions. Positional restraints were used only for zinc ion and its coordination sphere (including the side-chains of Cys473, His525, Cys535 and the crystallographic water molecule W1) to ensure a correct coordination geometry during simulation.

For each system three independent simulations (A1-A3 runs of 50 ns each; B1-B3 runs of at least 10 ns each) were performed by varying the seed used in the generation of random initial velocities of atoms [32]. The analysis and visualization of the MD trajectories were carried out using GROMACS [27] tools and PyMOL (The PyMOL Molecular Graphics System, Version 2.0 Schrödinger, LLC) program.

The calculation and visualization of protein cavities and tunnels were performed using CAVER 3.0.3 PyMOL plugin [33] with default settings. The crystallographic structures of Zn-R3 subunit (this work) and CS_2 hydrolase from *Acidianus* A1-3 (pdb code 3TEN) [34] were used. The structures were protonated and the position of the zinc ion was specified as starting point coordinate for calculation.

2.4. CS_2 hydrolase activity measurements

The CS_2 hydrolase activity of the purified Zn-R3 and Cd-R3 was monitored qualitatively by adding samples to airtight vials containing 200 μL of 40 mM HEPES buffer, pH 8.0 and 10 mM Pb(II) acetate. CS_2 in DMSO was added to the vials by syringe injection up to a 10 mM final concentration and the system incubated for 30 min at 25 °C. Pb(II) acetate precipitated over time did not negatively influence the activity tests. α- and β-CAs (bCA and FbiCA, respectively) [35,36] were also qualitatively tested. CS_2H used as control was incubated with CS_2 for 5 min at 50 °C in 20 mM HEPES buffer, pH 7.0 and 10 mM Pb(II) acetate [20]. In the wells containing active enzymes, the produced H_2S formed a clearly visible brown/black PbS precipitate.

CS_2 hydrolase activities of Zn-R3, Cd-R3, bCA and FbiCA were quantified by the methylene blue assay [37,38]. CS_2H was used as a control. 5 – 600 μg protein was added to airtight vials containing 200 μL of 40 mM HEPES buffer pH 8.0 and 1 mM zinc acetate (20 mM HEPES buffer, pH 7.0 was used as buffer for CS_2H). After 5 min preincubation, CS_2 in DMSO was added to the vials up to a 10 mM final concentration. The spontaneous rate of CS_2 hydrolysis was accounted by using enzyme free incubations with all other components present in the same amount. The kinetics of CS_2 hydrolase activity was worked out by testing 1 to 45 min enzyme/-substrate incubation time. The effect of the CA inhibitor (CAI) acetazolamide (AAZ) on H_2S production rate was determined by a CAI/enzyme 15 min preincubation prior to the substrate addition. The incubation with CS_2 was terminated by adding to the airtight vials a solution containing N,N-dimethylphenylenediamine and iron trichloride in HCl, that form methylene blue (MB) in the presence of hydrogen sulfide [37,38]. After 30 min at 25 °C, the absorbance of the solutions was measured at 748 nm (maximum absorption peak of the MBH_2^+ species of MB) using a Varian Cary 300 UV–Visible spectrophotometer. Calibration curves were prepared by dilution of freshly prepared sodium sulfide stock solution into 40 mM HEPES buffer pH 8.0 (or 20 mM HEPES buffer, pH 7.0 was used as buffer for CS_2H) containing 1 mM zinc acetate and the formation of MB was determined as previously stated [37,38]. Enzyme incubations in absence of Zn(II) lowered the MB formation as it is crucial to trap sulphide as the insoluble zinc sulfide, thus reducing the loss of sulfide by volatilization or oxidation.

3. Results

3.1. Crystallographic studies

Due to the difficulties to crystallize the full-length protein [14], in order to identify the CO_2 binding site crystallographic experiments were carried out on the single R3 repeat containing Zn(II),

hereafter indicated as Zn-R3, both in the unbound and in the substrate bound form. To this aim, the protein was crystallized by the hanging-drop method. The enzyme-substrate complex was then prepared by pressurizing one of these crystals with CO_2 for 5 min at 3 bar [9]. Pressurization with CO_2 was expected to have a double effect: *i*) to supply high concentration of substrate to the enzyme; *ii*) to decrease the pH value in the crystal as a consequence of the spontaneous reaction of carbon dioxide with water, which inactivates the enzyme and blocks the reaction (the enzyme is catalytically inefficient at low pH values) [9]. Data collection and refinement of the structures were carried out as described in the experimental section.

Fig. 2 reports the comparison of the active sites of Zn-R3 with and without CO_2 bound. When the substrate is not present in the active site (Fig. 2A), in agreement with what observed for Zn-R2 [2] the metal ion is coordinated in a tetrahedral geometry by the three conserved protein residues Cys473, His525 and Cys535 and a water molecule (W1). The latter is in turn hydrogen bonded to a second water molecule (W2) and to the conserved residues Gly536 and Asp475. CO_2 binds within the active site without altering the metal ion coordination geometry but only displacing the water molecule W2 (Fig. 2B and 2C). It resides in a hydrophobic pocket delimited by residues Val474, Phe537, Phe603, Thr627, Leu631 (Fig. 2D), with the zinc-bound water molecule nearly equidistant from both CO_2 oxygens (with distances of 3.0 and 3.3 Å, respectively) and at 2.9 Å from the CO_2 carbon atom which is ready to undergo the nucleophilic attack. A further hydrogen bond interaction between one of the two carbon dioxide oxygens and Phe537N atom further stabilizes the substrate binding (Fig. 2B).

3.2. Molecular dynamics simulations

Once identified the CO_2 binding site, the entry route for the substrate to the active site was also investigated by means of all-atom molecular dynamics (MD) simulations in explicit solvent. MD simulations have been widely used to investigate ligand migration paths inside proteins, also in the case of CO_2 ligand [39–41] but little is known on this topic for CAs, apart from few MD studies on hCA II isoform [42–44]. As first step, we employed CAVER program [33] to identify tunnels inside the protein, using the here reported X-ray structure of Zn-R3. This analysis reveals two routes leading to the bulk solvent from the active site. The first one is represented by a shallow cleft (displayed in blue in Fig. 3) and the second one is a long and narrow L-shaped tunnel (indicated in red in Fig. 3).

In order to investigate which one was the migration pathway of CO_2 inside the protein, we performed MD simulations using the crystallographic coordinates of the enzyme/CO_2 complex as a starting structure. Three independent runs (A1-A3) of 50 ns were carried out to enhance MD sampling. In the following, we will refer to results concerning A1, whereas results from the other two trajectories are shown in Supplementary Information (Figs. S2-S3). In all the simulations, CO_2 molecule migrates from the active site toward the exterior of the protein *via* the narrow L-shaped tunnel, which is lined by hydrophobic residues (Fig. 4A). In contrast, the shallow cleft was explored only for a very short time in A1 run. Fig. 4B reports the distance between the zinc ion and the carbon atom of the CO_2 molecule during simulation as a function of time for A1 run. At the beginning of the simulation CO_2 molecule leaves the crystallographic binding site and quickly returns to it after exploring the shallow cleft for 2 ns. Then, at approximately 3.5 ns, CO_2 molecule enters the hydrophobic tunnel and rapidly passes through it (position **1*** and **2***, at C-Zn distance of 8–9 Å and 13–14 Å, respectively), reaching its external border placed at a C-Zn distance of around 18 Å (position **3*** in Fig. 4B). The molecule remains there for few nanoseconds, then it comes back to the tunnel interior (position **2*** and **1***), and finally moves to the external border again, so on till 41 ns when it definitely goes out of the protein. Thus, during the entire trajectory, the CO_2 molecule oscillates between the interior of the tunnel and its external border, probably due to the high affinity toward the residues delimiting the internal part of the tunnel. In particular, it preferentially resides into hydrophobic pockets placed at a distance of 9, 14 and 18 Å from the zinc ion (corresponding to positions **1***-**3*** in Fig. 4B). Very similar results were obtained from A2 and A3 trajectories (Fig. S2-S3). Some snapshots extracted from A1 trajectory and representing the CO_2 molecule moving through preferential pockets **1***, **2*** and **3*** and finally out of the tunnel are depicted in Fig. 4C-F, whereas protein residues interacting with it in these pockets are listed in Table S2. Within the tunnel CO_2 interacts with protein residues mainly through van der Waals interactions; these interactions are strong enough to facilitate CO_2 entrance and migration, but not tight enough to allow its binding and trapping and thus hamper the enzymatic turnover. It is worth noting that along the trajectory, the molecule suddenly exits and rapidly enters again through the tunnel entrance at approximately 20 ns (Fig. 4B), thus suggesting that the tunnel entrance is the route for the substrate to enter the protein and reach the active site.

To confirm this hypothesis, three additional MD simulations (B1-B3) were performed placing the CO_2 molecule at the exterior of the protein, at 5 Å distance from the tunnel entrance (Fig. S1). In two of the three simulations, the molecule enters the tunnel and reaches the active site (results concerning B1 are shown in Fig. 5, whereas results concerning B2 are reported in Fig. S4). Again, these simulations indicate that CO_2 has a high affinity for the hydrophobic tunnel residues and migrates along the tunnel oscillating between the interior of the tunnel and its external border occupying the pockets **1***, **2*** and **3*** already encountered in A1-A3 trajectories.

All together, these MD simulations clearly indicate the long L-shaped hydrophobic tunnel as the entry route for the CO_2 substrate of R3 active site. Interestingly, considering the structural model of CDCA full-length protein [14] the tunnel is accessible to the substrate in all the three subunits (R1, R2 and R3) (Fig. S5), further supporting the hypothesis of the tunnel as a reliable entry route for CO_2.

3.3. Enzymatic assays

A long, highly hydrophobic tunnel providing access to the active site, similar to that identified in Zn-R3 by MD simulations, was already observed in a functionally related enzyme, namely the CS_2 hydrolase from *Acidianus* A1-3 (Fig. S6) [20]. This is a rather peculiar enzyme since, although possessing an active site and a three dimensional structure similar to those of β-CAs, it is not able to catalyze the carbon dioxide hydration reaction, but only the conversion of CS_2 to H_2S with COS as intermediate: $CS_2 + H_2O \rightarrow COS + H_2S$ and $COS + H_2O \rightarrow CO_2 + H_2S$. This substrate specificity was ascribed to the presence of a very hydrophobic tunnel, which shows great affinity for highly hydrophobic substrates such as CS_2 and COS. Driven by this similarity, we decided to investigate the capability of CDCA1 to catalyze the CS_2 conversion reaction. Again, we used purified Zn-R3 as model enzyme for our experiments, following an experimental procedure previously described in literature [37,38]. The development of H_2S was detected qualitatively by the formation of lead sulfide and quantified by the widely used methylene blue assay [37,38]. For comparison, enzymatic assays were also conducted on bovine CA (bCA) [35] and on a plant

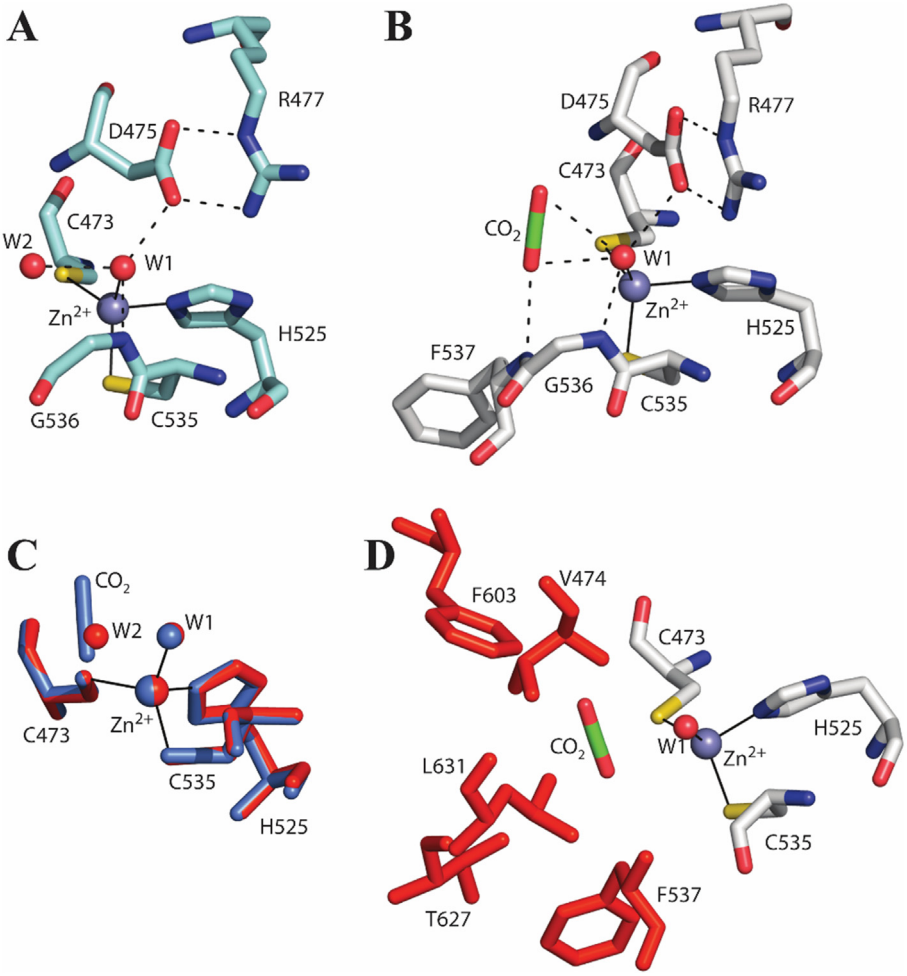

Fig. 2. Zn-R3 active site. (A) Stick representation of Zn-R3; (B) Stick representation of Zn-R3/CO_2; (C) Structural superposition of Zn-R3 (red) and Zn-R3/CO_2 (blue) active sites; (D) CO_2 binding pocket (highlighted in red) in Zn-R3/CO_2 active site. Zinc coordinating residues, CO_2, and residues constituting the CO_2 binding pocket are reported as sticks, whereas zinc ion and water molecules are reported as spheres. (For interpretation of the references to colour in this figure legend, the reader is referred to the web version of this article.)

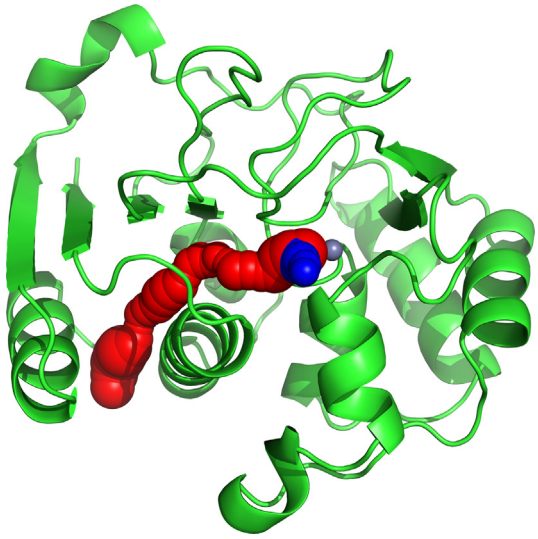

Fig. 3. Tunnels identified in Zn-R3 using CAVER [33]. The protein is shown as green cartoon and individual tunnels are represented by a sequence of spheres with variable radii. The shallow cleft is shown in blue, the long narrow tunnel is in red. Zn^{2+} ion is displayed as a grey sphere. (For interpretation of the references to colour in this figure legend, the reader is referred to the web version of this article.)

CA (FbiCA from *Flaveria bidentis)* [36] which belong to the α- and β-classes, respectively. CS_2 hydrolase from *Sulfolobus solfataricus* (CS_2H) was used as a positive control [20].

To verify the CS_2 hydrolase activity of Zn-R3, several enzyme concentrations were tested with a constant CS_2 concentration, proximal to its water solubility. Significant H_2S production was detected with a Zn-R3 concentration of 10^{-5} M, which reached a plateau after 45 min. (Fig. 6A, red line). Surprisingly, when the same concentration was used for the R3 repeat containing Cd (hereafter indicated as Cd-R3) a much lower activity was observed (Fig. 6A, blue line). Indeed, H_2S produced by 10^{-5} M Cd-R3 after 45 min was even lower than the amount produced by 10^{-6} M Zn-R3 after the same time (Fig. 6B). H_2S produced by 10^{-6} M Cd-R3 after 45 min could be barely detected. Very low activity was observed also for bCA up to a concentration of 10^{-4} M (Fig. 6B), whereas a similar FbiCA concentration produced no H_2S at all, after the same time. It is noteworthy that the CS_2 hydrolase activity of Zn-R3 was 70% inhibited by an equimolar amount of the zinc-binder CA inhibitor acetazolamide (AAZ) (Fig. 6C). These data clearly indicate that, differently from other CA enzymes so far studied, CDCA1 catalyzes also the CS_2 hydrolysis reaction when zinc is present in the active site, and that this activity, similarly to the CO_2 hydration, is inhibited by AAZ [14]. The CS_2 conversion to H_2S catalyzed by Zn-R3 was found to be significantly slower in

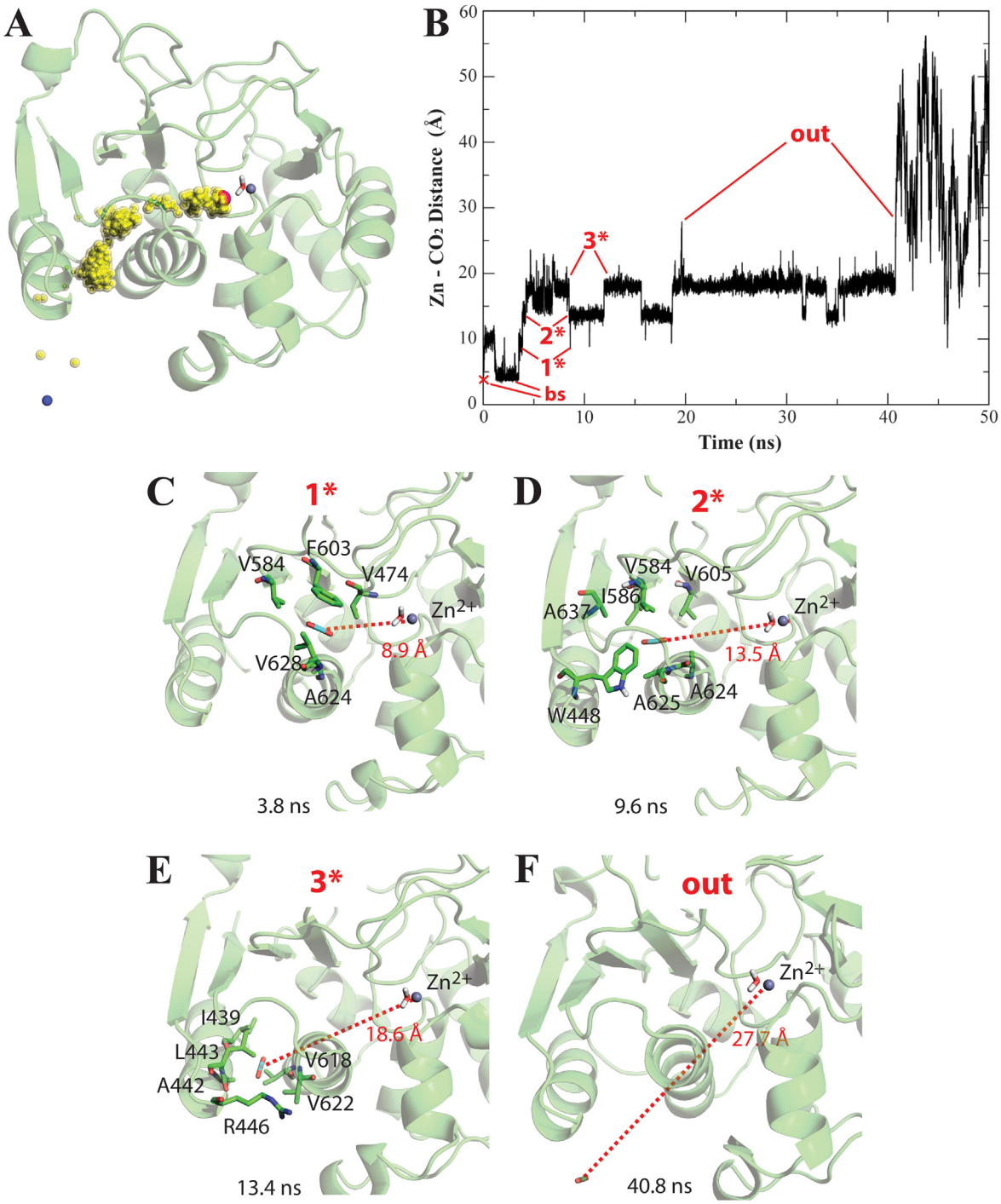

Fig. 4. CO_2 migration from R3 active site in A1 run. (A) Displacement of CO_2 carbon atom (yellow spheres) as it moves from the active site in A1 simulation. The starting and final (41 ns) position of CO_2 molecule is indicated by red and blue spheres, respectively. Zn^{2+} ion is shown as a grey sphere and Zn^{2+}-coordinating water molecule is shown in stick representation. (B) Distance between Zn^{2+} ion and the CO_2 carbon atom during A1 run plotted as a function of time. Pockets (1*, 2*, 3*) corresponding to CO_2 positions are indicated. bs corresponds to CO_2 position in the binding site, according to the crystallographic structure. The red cross indicates the beginning of the simulation, when CO_2 is in its binding site. (C-F) Snapshots extracted during A1 simulation. CO_2 molecule and amino acids interacting with it in pockets 1*, 2* and 3* are displayed in stick representation. (For interpretation of the references to colour in this figure legend, the reader is referred to the web version of this article.)

comparison to that catalyzed by the positive control CS_2H which has CS_2 as its main substrate. In fact, H_2S produced by 10^{-5} M Zn-R3 after 45 min was approximately half the quantity generated by 10^{-6} M CS_2H after 5 min (Fig. 6D).

4. Discussion

Since its discovery, CDCA1 demonstrated to be a rather peculiar enzyme with respect to other CAs previously identified. Indeed, it

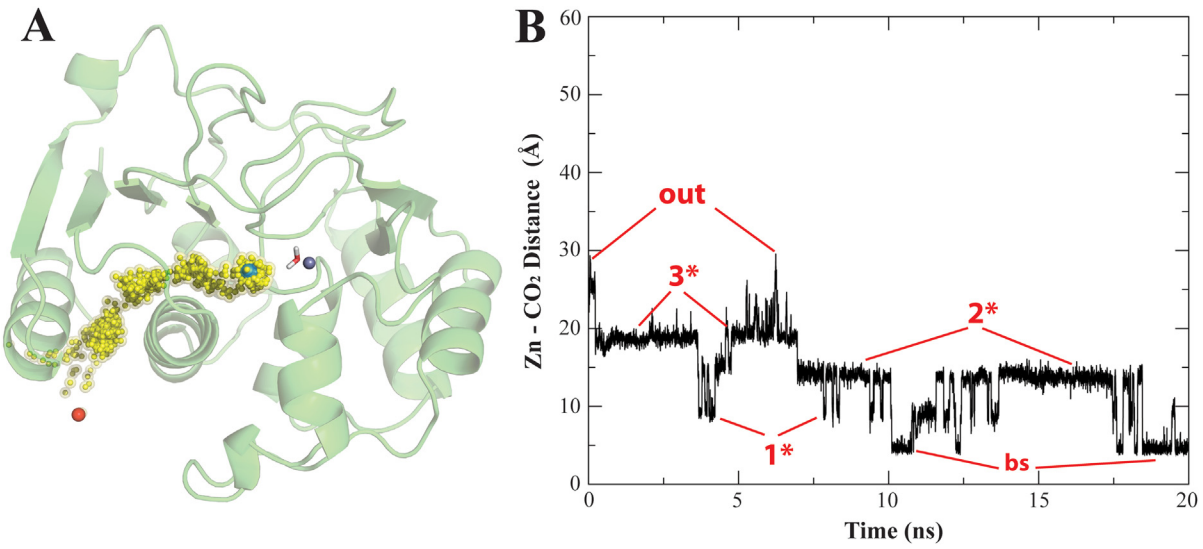

Fig. 5. CO_2 entering and migration to the R3 active site in B1 run. (A) Displacement of CO_2 carbon atom (yellow spheres) as it moves from the exterior of the protein to the active site. The starting (0 ns) and final (20 ns) position is indicated by red and blue spheres, respectively. (B) Distance between Zn^{2+} ion and the CO_2 carbon atom during B1 run plotted as a function of time. Pockets (1*, 2*, 3*) corresponding to CO_2 positions are indicated. bs corresponds to CO_2 position in its binding site, according to the crystallographic structure. (For interpretation of the references to colour in this figure legend, the reader is referred to the web version of this article.)

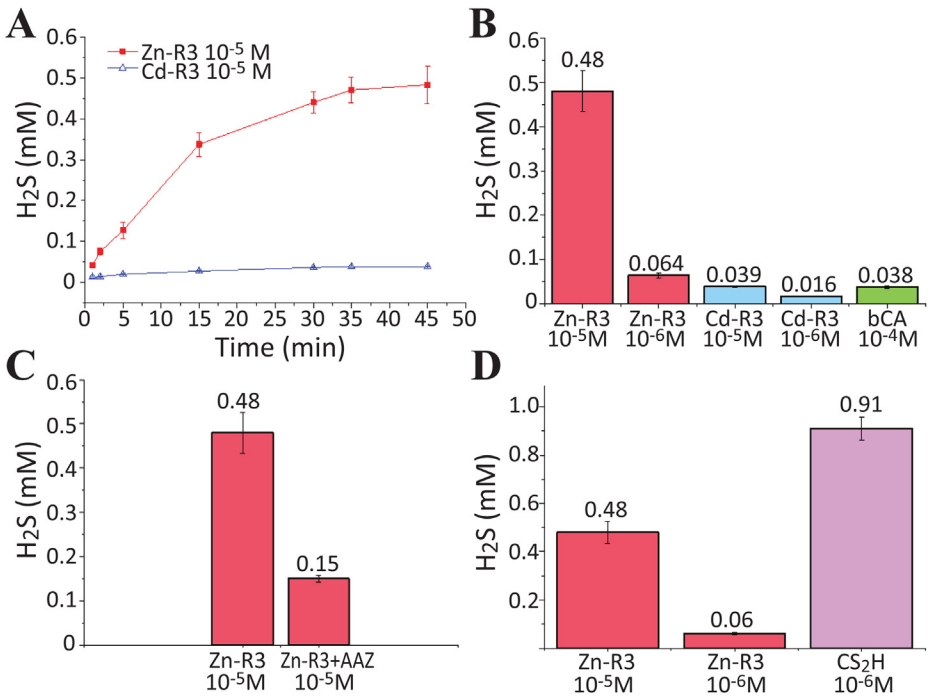

Fig. 6. CS_2 hydrolase activity of R3. (A) Time-dependent H_2S release of 10^{-5} M Zn-R3 (red squares) and 10^{-5} M Cd-R3 (blue triangles) with a 10 mM substrate concentration. (B) Released H_2S concentration after 45 min incubation at 25 °C by 10^{-5} and 10^{-6} M R3 enzymes and 10^{-4} M bCA. (C) Inhibition of the Zn-R3 enzyme by equimolar AAZ. (D) Comparison of Zn-R3 H_2S production (after 45 min incubation at 25 °C) with that of 10^{-6} M CS_2H from *S. solfataricus* at 50 °C after 5 min. The reported values are mean from 3 different assays, errors are in the range of ± 3–15% of the reported values. (For interpretation of the references to colour in this figure legend, the reader is referred to the web version of this article.)

has been the first enzyme to show an efficient utilization of Cd(II) ions in Nature [45–47] in addition to a unique adaptation capability to live on the surface ocean. In this environment, which is extremely depleted in essential metal ions [48] CDCA1 utilizes Zn(II) or Cd(II) as catalytic metal to support the metabolic needs of fast growing diatoms [2].

Despite these features, the existing studies on CDCA1 are limited with few information on its catalytic mechanism. To fill this gap, we have undertaken a detailed characterization of this enzyme by using a multidisciplinary approach. First, we have determined the structure of Zn-R3 CDCA1 in complex with CO_2 substrate, identifying for the first time the CO_2 binding site of a ζ-class CA enzyme. Interestingly, despite the absence of any structural similarity between α- and ζ-CAs, the CO_2 binding in Zn-R3 presents several common features with the CO_2 binding in α-class hCA II [9,12] such as the distances between the zinc-bound

solvent molecule and the three carbon dioxide atoms, as well as the presence of an hydrophobic pocket, where the substrate molecule can accommodate (Fig. 7A). Even more similarities are present when comparing the CO_2 binding site in β-CAs (Fig. 7B and 7C). In this case, the three metal-coordinating residues as well as the catalytic dyad Asp/Arg, which in β-CAs is supposed to help the stabilization of the zinc bound nucleophile [49] are conserved, whereas the two CO_2 binding pockets are spatially superimposable (Fig. 7C). Once again CAs demonstrated to be an excellent example of convergent evolution, where three different structural architectures (α-, β, and ζ-CAs) share a very similar organization of the catalytic site and mechanism [50].

By using MD simulations, we identified the CO_2 access route to the active site of CDCA1 enzyme, which consists in a narrow, long and highly hydrophobic tunnel (Fig. 4A). In this case, an important difference is observed with respect to data reported for α- and β-CAs. Indeed, MD simulations carried out for α-class hCA II identified a quite large cavity spanning from the protein surface to the active site as the CO_2 access route of this enzyme. This cavity consists of both hydrophobic and hydrophilic residues that delineate two very different environments (Fig. S7A) [51,52]. It has been suggested that hydrophobic residues are used to entrap the CO_2 molecule, while hydrophilic ones allows the release of the polar reaction products (bicarbonate and proton) [53]. No MD studies on the CO_2 access route have been reported for β-CAs so far; however, hypotheses on the substrate entry route have been formulated based on crystallographic results [54] which identified a funnel shaped cavity as possible CO_2 migration pathway. Again, as observed for hCA II, this cavity contains both hydrophobic and hydrophilic residues (Fig. S7B). Thus, the presence of a narrow, long and highly hydrophobic tunnel as substrate entry route seems to be a unique feature of ζ-CAs with respect to the other canonical CA-classes for which this feature has been investigated. On the contrary, such peculiarity was observed in a class of CA related enzymes, namely CS_2 hydrolases. Starting from this similarity, we hypothesized and then demonstrated by enzymatic assays that, beyond its classical CA activity, CDCA1 is also able to catalyze the conversion of CS_2 to H_2S with COS as intermediate. This is a particularly fascinating result considering that CDCA1 is the unique enzyme, known so far, able to use both CS_2 and CO_2 as substrates. Indeed, whereas COS has been demonstrated to be a substrate for plant and algal CAs [55,56] and for the CA of the flour beetle *Tribolium castaneaum* [37], no experimental evidence of a CA able to catalyze the CS_2 conversion has been provided so far. Analogously, CO_2 is not a substrate of CS_2 hydrolase, the enzyme whose main function is CS_2 conversion [20]. It is worth noting that the absence of a significant CS_2 hydrolase activity for β- and α-CAs is in line with our structural analysis that highlights the absence in these enzymes of a highly hydrophobic tunnel necessary to allow the entrance and migration of a highly hydrophobic substrate as CS_2.

The physiological implications of this supplementary catalytic activity still remain to be unveiled. We suggest here that this could represent another ability of diatoms expressing CDCA1 to adapt to the external environment. It is known that CS_2 is present in marine environments as a breakdown product from organic matter, mainly dimethyl sulfide [34,57]. The ability of this enzyme to convert CS_2 could represent an alternative source of carbon acquisition for diatoms, in addition to CO_2. This hypothesis is in line with a study reported by Walsh and coworkers showing that some phytoplankton species, among which *Thalaissosira oceanica* which expresses a CDCA1-like enzyme [58] produce hydrogen sulfide in the surface ocean [59]. In this context, the different CDCA1 capability to catalyze CS_2 conversion when zinc or cadmium are present in the active site, could be a regulation mechanism to switch from one to the other metabolic activity.

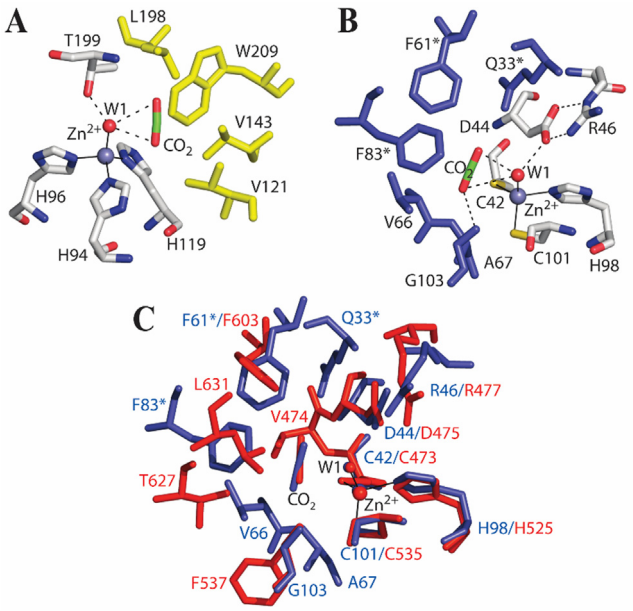

Fig. 7. CO_2 binding site in CAs. Stick representation of the CO_2 binding pocket in (A) α-CAs (hCA II, PDB code 2VVA) [9] and (B) β-CAs (psCA3, PDB code 5BQ1) [10]; (C) Structural superposition of β-CA (blue) and ζ-CA (red) active sites. Zinc coordinating residues, CO_2, catalytic dyad Asp/Arg and residues constituting the CO_2 binding pocket are reported as sticks, whereas Zn^{2+} ion and its coordinating water molecule are reported as spheres. (For interpretation of the references to colour in this figure legend, the reader is referred to the web version of this article.)

In conclusion, we demonstrate here a further catalytic versatility of the fascinating ζ-CA class, by using a combination of X-ray crystallographic, computational and enzymatic experiments. Apart from dissecting and explaining in detail the way in which the small molecule gaseous substrate CO_2 travels from the environment to the active site of CDCA1, where it binds in a hydrophobic pocket similar to that of other CA classes, we demonstrate that also CS_2 is a substrate for this enzyme. This finding is new and unexpected as until now only few CS_2 hydrolases have been characterized, and none of them is reported to have any CO_2 hydratase action. Our investigations may also explain why diatoms, which are organisms where many CA classes co-exist, are on one hand rich in these biologic catalysts and, on the other one, able to survive in limiting conditions, adapting to a switch in the use of different metal ion cofactors (zinc *versus* cadmium) or substrates for carbon acquisition (CO_2 *versus* CS_2), thus making them one of the most versatile organisms present in Nature, in addition of being the organisms that furnish 80% of the oxygen that we breath.

Author contributions

VA, CTS, SMM and GDS, designed research; VA, EL, MB, DE, AN, EB, SB and MP performed research; GDS wrote the paper.

CRediT authorship contribution statement

Vincenzo Alterio: Conceptualization, Methodology, Investigation. **Emma Langella:** Investigation. **Martina Buonanno:** Investigation. **Davide Esposito:** Investigation. **Alessio Nocentini:** Investigation. **Emanuela Berrino:** Investigation. **Silvia Bua:** Investigation. **Maurizio Polentarutti:** Investigation. **Claudiu T. Supuran:** Conceptualization, Methodology. **Simona Maria Monti:** Conceptualization, Methodology. **Giuseppina De Simone:** Conceptualization, Methodology.

Declaration of Competing Interest

The authors declare that they have no known competing financial interests or personal relationships that could have appeared to influence the work reported in this paper.

Acknowledgement

We thank Mr. Maurizio Amendola and Mr. Luca De Luca for technical support.

Funding

This work was supported by MUR (grant FISR2019_04819 BacCAD).

Appendix A. Supplementary data

Supplementary data to this article can be found online at https://doi.org/10.1016/j.csbj.2021.05.057.

References

[1] Supuran CT, De Simone G, editors. Carbonic Anhydrases as Biocatalysts. From Theory to Medical and Industrial Applications. The Netherlands: Elsevier; 2015.
[2] Xu Y, Feng L, Jeffrey PD, Shi Y, Morel FM. Structure and metal exchange in the cadmium carbonic anhydrase of marine diatoms. Nature 2008;452 (7183):56–61.
[3] Del Prete S, Vullo D, Fisher GM, Andrews KT, Poulsen SA, Capasso C, et al. Discovery of a new family of carbonic anhydrases in the malaria pathogen Plasmodium falciparum–the eta-carbonic anhydrases. Bioorg Med Chem Lett 2014;24(18):4389–96.
[4] Kikutani S, Nakajima K, Nagasato C, Tsuji Y, Miyatake A, Matsuda Y. Thylakoid luminal theta-carbonic anhydrase critical for growth and photosynthesis in the marine diatom Phaeodactylum tricornutum. Proc Natl Acad Sci U S A 2016;113 (35):9828–33.
[5] Ferry JG. The gamma class of carbonic anhydrases. Biochim Biophys Acta 2010;1804(2):374–81.
[6] Sawaya MR, Cannon GC, Heinhorst S, Tanaka S, Williams EB, Yeates TO, et al. The structure of beta-carbonic anhydrase from the carboxysomal shell reveals a distinct subclass with one active site for the price of two. J Biol Chem 2006;281(11):7546–55.
[7] Alterio V, Di Fiore A, D'Ambrosio K, Supuran CT, De Simone G. Multiple binding modes of inhibitors to carbonic anhydrases: how to design specific drugs targeting 15 different isoforms?. Chem Rev 2012;112(8):4421–68.
[8] Jensen EL, Clement R, Kosta A, Maberly SC, Gontero B. A new widespread subclass of carbonic anhydrase in marine phytoplankton. Isme J 2019;13 (8):2094–106.
[9] Sjoblom B, Polentarutti M, Djinovic-Carugo K. Structural study of X-ray induced activation of carbonic anhydrase. Proc Natl Acad Sci U S A 2009;106 (26):10609–13.
[10] Aggarwal M, Chua TK, Pinard MA, Szebenyi DM, McKenna R. Carbon Dioxide "Trapped" in a beta-Carbonic Anhydrase. Biochemistry 2015;54(43):6631–8.
[11] Schlicker C, Hall RA, Vullo D, Middelhaufe S, Gertz M, Supuran CT, et al. Structure and inhibition of the CO2-sensing carbonic anhydrase Can2 from the pathogenic fungus Cryptococcus neoformans. J Mol Biol 2009;385 (4):1207–20.
[12] Domsic JF, Avvaru BS, Kim CU, Gruner SM, Agbandje-McKenna M, Silverman DN, et al. Entrapment of carbon dioxide in the active site of carbonic anhydrase II. J Biol Chem 2008;283(45):30766–71.
[13] Lane TW, Saito MA, George GN, Pickering IJ, Prince RC, Morel FM. Biochemistry: a cadmium enzyme from a marine diatom. Nature 2005;435 (7038):42.
[14] Alterio V, Langella E, Viparelli F, Vullo D, Ascione G, Dathan NA, et al. Structural and inhibition insights into carbonic anhydrase CDCA1 from the marine diatom Thalassiosira weissflogii. Biochimie 2012;94(5):1232–41.
[15] Innocenti A, Supuran CT. Paraoxon, 4-nitrophenyl phosphate and acetate are substrates of alpha- but not of beta-, gamma- and zeta-carbonic anhydrases. Bioorg Med Chem Lett 2010;20(21):6208–12.
[16] Viparelli F, Monti SM, De Simone G, Innocenti A, Scozzafava A, Xu Y, et al. Inhibition of the R1 fragment of the cadmium-containing zeta-class carbonic anhydrase from the diatom Thalassiosira weissflogii with anions. Bioorg Med Chem Lett 2010;20(16):4745–8.
[17] Angeli A, Buonanno M, Donald WA, Monti SM, Supuran CT. The zinc - but not cadmium - containing zeta-carbonic from the diatom Thalassiosira weissflogii is potently activated by amines and amino acids. Bioorg Chem 2018;80:261–5.
[18] Supuran CT, Nocentini A, editors. Carbonic Anhydrases, Biochemistry and Pharmacology of en Evergreen Pharmaceutical Target. London, UK: Elsevier; 2019.
[19] Alterio V, Langella E, De Simone G, Monti SM. Cadmium-containing carbonic anhydrase CDCA1 in marine diatom Thalassiosira weissflogii. Mar Drugs 2015;13(4):1688–97.
[20] Smeulders MJ, Barends TR, Pol A, Scherer A, Zandvoort MH, Udvarhelyi A, et al. Evolution of a new enzyme for carbon disulphide conversion by an acidothermophilic archaeon. Nature 2011;478(7369):412–6.
[21] Otwinowski Z, Minor W. Processing of X-ray diffraction data collected in oscillation mode. Methods Enzymol 1997;276:307–26.
[22] Navaza J, Saludjian P. [33] AMoRe: An automated molecular replacement program package. Methods Enzymol 1997;276:581–94.
[23] Brunger AT. Version 1.2 of the Crystallography and NMR system. Nat Protoc 2007;2(11):2728–33.
[24] Brunger AT, Adams PD, Clore GM, DeLano WL, Gros P, Grosse-Kunstleve RW, et al. Crystallography & NMR system: A new software suite for macromolecular structure determination. Acta Crystallogr D Biol Crystallogr 1998;54(Pt 5):905–21.
[25] Jones TA, Zou JY, Cowan SW, Kjeldgaard M. Improved methods for building protein models in electron density maps and the location of errors in these models. Acta Crystallogr A 1991;47(Pt 2):110–9.
[26] Djinovic-Carugo K, Everitt P, Tucker PA. A cell for producing xenon-derivative crystals for cryocrystallographic analysis. J Appl Crystallogr 1998;31:812–4.
[27] Van Der Spoel D, Lindahl E, Hess B, Groenhof G, Mark AE, Berendsen HJ. GROMACS: fast, flexible, and free. J Comput Chem 2005;26(16):1701–18.
[28] Sousa da Silva AW, Vranken WF. ACPYPE - AnteChamber PYthon Parser interfacE. BMC Res Notes 2012;5:367.
[29] Hess B, Bekker H, Berendsen HJC, Fraaije JGEM. LINCS: A linear constraint solver for molecular simulations. J Comput Chem 1997;18(12):1463–72.
[30] Darden T, York D, Pedersen L. Particle Mesh Ewald - an N. Log(N) Method for Ewald Sums in Large Systems. J Chem Phys 1993;98(12):10089–92.
[31] Darden T, Perera L, Li LP, Pedersen L. New tricks for modelers from the crystallography toolkit: the particle mesh Ewald algorithm and its use in nucleic acid simulations. Struct Fold Des 1999;7(3):R55–60.
[32] Negureanu L, Salsbury FR. Insights into Protein - DNA Interactions, Stability and Allosteric Communications: A Computational Study of Muts alpha-DNA Recognition Complexes. J Biomol Struct Dyn 2012;29(4):757–76.
[33] E. Chovancova A. Pavelka P. Benes O. Strnad J. Brezovsky B. Kozlikova et al. CAVER 3.0: a tool for the analysis of transport pathways in dynamic protein structures PLoS Comput Biol 2012;8(10):e1002708.
[34] Smeulders MJ, Pol A, Venselaar H, Barends TR, Hermans J, Jetten MS, et al. Bacterial CS2 hydrolases from Acidithiobacillus thiooxidans strains are homologous to the archaeal catenane CS2 hydrolase. J Bacteriol 2013;195 (18):4046–56.
[35] Demir Y, Demir N, Nadaroglu H, Bakan E. Purification and characterization of carbonic anhydrase from bovine erythrocyte plasma membrane. Prep Biochem Biotechnol 2000;30(1):49–59.
[36] Dathan NA, Alterio V, Troiano E, Vullo D, Ludwig M, De Simone G, et al. Biochemical characterization of the chloroplastic beta-carbonic anhydrase from Flaveria bidentis (L.) "Kuntze". J Enzyme Inhib Med Chem 2014;29 (4):500–4.
[37] Haritos VS, Dojchinov G. Carbonic anhydrase metabolism is a key factor in the toxicity of CO2 and COS but not CS2 toward the flour beetle Tribolium castaneum [Coleoptera: Tenebrionidae]. Comp Biochem Physiol C Toxicol Pharmacol 2005;140(1):139–47.
[38] Reese BK, Finneran DW, Mills HJ, Zhu MX, Morse JW. Examination and Refinement of the Determination of Aqueous Hydrogen Sulfide by the Methylene Blue Method. Aquat Geochem 2011;17(4–5):567–82.
[39] Karmakar T, Periyasamy G, Balasubramanian S. CO2 Migration Pathways in Oxalate Decarboxylase and Clues about Its Active Site. J Phys Chem B 2013;117 (41):12451–60.
[40] Drummond ML, Wilson AK, Cundari TR. Nature of Protein-CO2 Interactions as Elucidated via Molecular Dynamics. J Phys Chem B 2012;116(38):11578–93.
[41] Drummond ML, Wilson AK, Cundari TR. Carbon Dioxide Migration Pathways in Proteins. J Phys Chem Lett 2012;3(7):830–3.
[42] Chen G, Kong XA, Lu DN, Wu JZ, Liu Z. Kinetics of CO2 diffusion in human carbonic anhydrase: a study using molecular dynamics simulations and the Markov-state model. Phys Chem Chem Phys 2017;19(18):11690–7.
[43] Liang JY, Lipscomb WN. Binding of Substrate Co2 to the Active-Site of Human Carbonic Anhydrase-Ii - a Molecular-Dynamics Study. Proc Natl Acad Sci U S A 1990;87(10):3675–9.
[44] Merz KM. Carbon dioxide binding to human carbonic anhydrase II. J Am Chem Soc 1991;113:6.
[45] Lane TW, Morel FM. A biological function for cadmium in marine diatoms. Proc Natl Acad Sci U S A 2000;97(9):4627–31.
[46] Chmielowska-Bak J, Izbianska K, Deckert J. The toxic Doppelganger: on the ionic and molecular mimicry of cadmium. Acta Biochim Pol 2013;60 (3):369–74.
[47] Belyaeva EA, Dymkowska D, Wieckowski MR, Wojtczak L. Mitochondria as an important target in heavy metal toxicity in rat hepatoma AS-30D cells. Toxicol Appl Pharmacol 2008;231(1):34–42.
[48] Morel FMM, Milligan AJ, Saito MA. Marine Bioinorganic Chemistry: The Role of Trace Metals in the Oceanic Cycles of Major Nutrients. Treatise on Geochemistry 2003;6:31.

[49] Kimber MS, Pai EF. The active site architecture of Pisum sativum beta-carbonic anhydrase is a mirror image of that of alpha-carbonic anhydrases. Embo J 2000;19(7):1407–18.
[50] Liljas A, Laurberg M. A wheel invented three times. The molecular structures of the three carbonic anhydrases. EMBO Rep 2000;1(1):16–7.
[51] Liang JY, Lipscomb WN. Binding of substrate CO2 to the active site of human carbonic anhydrase II: a molecular dynamics study. Proc Natl Acad Sci U S A 1990;87(10):3675–9.
[52] De Simone G, Alterio V, Supuran CT. Exploiting the hydrophobic and hydrophilic binding sites for designing carbonic anhydrase inhibitors. Expert Opin Drug Discov 2013;8(7):793–810.
[53] Maupin CM, Castillo N, Taraphder S, Tu C, McKenna R, Silverman DN, et al. Chemical rescue of enzymes: proton transfer in mutants of human carbonic anhydrase II. J Am Chem Soc 2011;133(16):6223–34.
[54] Teng YB, Jiang YL, He YX, He WW, Lian FM, Chen Y, et al. Structural insights into the substrate tunnel of Saccharomyces cerevisiae carbonic anhydrase Nce103. BMC Struct Biol 2009;9:67.
[55] Protoschill-Krebs G, Wilhelm C, Kesselmeier J. Consumption of carbonyl sulphide (COS) by higher plant carbonic anhydrase (CA). Atmos Environ 1996;30(18):6.
[56] Blezinger S, Wilhelm C, Kesselmeier J. Enzymatic consumption of carbonyl sulfide (COS) by marine algae. Biogeochemistry 2000;48:13.
[57] Watts SF. The mass budgets of carbonyl sulfide, dimethyl sulfide, carbon disulfide and hydrogen sulfide. Atmos Environ 2000;34(5):19.
[58] Park H, Song B, Morel FM. Diversity of the cadmium-containing carbonic anhydrase in marine diatoms and natural waters. Environ Microbiol 2007;9(2):403–13.
[59] Walsh RS, Cutter GA, Dunstan WM, Radford-Knoery J, Elder JT. The biogeochemistry of hydrogen sulfide: Phytoplankton production in the surface ocean. Limnol Oceanogr 1994;39(4).